Electronic Supplementary Material (ESI) for ChemComm.

Supplementary Information

A multi-chromic boron trifluoride-pyridyl Lewis adduct

Peter W. McDonald,[a] and Chris Ritchie.[a*]

a School of Chemistry, Monash University, Clayton, Victoria, Australia

Funding and acknowledgments

The authors acknowledge and thank Dr. Andrew D. Scully from CSIRO Manufacturing, Clayton, Victoria 3168, Australia for carrying out total PLQY and time-resolved luminescence measurements. The authors also thank Prof. Kellie Tuck and Dr. Rosemary Young from Monash University for technical assistance, and the Monash Chemistry team (Dr Alasdair McKay, Dr. Craig Forsyth, and Dr. Boujemaa Moubaraki). C.R. thanks Monash University and the ARC for funding this research (FT180100610). P.W.M. thanks Monash University and the Australian Government for a Research Training Program (RTP) Scholarship. The authors acknowledge the use of facilities within the Monash X-Ray Platform. There are no conflicts to declare.

*Email: chris.ritchie@monash.edu

Table of Contents

S1: Materials, instrumentation and methods

Chemicals

18-crown-6 (Sigma-Aldrich 99%), acetonitrile – ACN, (Merck Uvasol), 4-aminopyridine (Sigma-Aldrich 98%), boron trifluoride diethyl etherate (Merck), bromobenzene (Sigma-Aldrich reagent plus), copper(I) iodide (ChemSupply), dichloromethane – DCM, (Merck Uvasol), diethyl ether (Merck ACS grade), ethyl acetate anhydrous, 99.8% (Merck), magnesium sulphate anhydrous (Merck), methanol – MeOH, (Merck Uvasol), potassium carbonate anhydrous (ChemSupply AR), toluene – tol (Merck Uvasol). All reagents were used as received unless otherwise stated. Bromobenzene was dried using 3 Å sieves.

FT-IR spectroscopy

FT-IR spectroscopy was performed on an Agilent Cary 630 FTIR spectrometer. Samples were used neat. Signals are listed as wavenumbers (ν, cm^{-1}).

Elemental analysis

Elemental analysis was conducted by Dr Alasdair McKay using a Perkin Elmer 2400 Series II CHN Analyser. The detector was calibrated using Acetanilide on the day of use and each sample was collected in duplicate.

Nuclear magnetic resonance spectroscopy

^{1}H, ^{13}C, ^{11}B and ^{19}F NMR spectra were recorded at 298 K in dichloromethane-d_2 or acetonitrile-d_3 on either a Bruker Avance NEO NMR spectrometer equipped with a 9.4 T magnet and 5 mm BBO (926) probe, operating at 400 MHz (^{1}H), 376 MHz (^{19}F) and 128 MHz (^{11}B) or a Bruker Avance III NMR spectrometer equipped with a 14.1 T magnet and TCI cryoprobe, operating at 600 MHz (^{1}H) and 151 MHz (^{13}C). Chemical shifts (δ) are reported in ppm and were referenced to the residual solvent signals (^{1}H, ^{13}C). Bruker software, TopSpin 3.6.1 and Mnova 14.2.3 were used for data acquisition and processing.

Single Crystal X-ray diffraction

Low-temperature (123 K) and ambient temperature (293 K) X-ray intensity data for **1-BF_3** and **1H-BF_4** were collected using a Rigaku Oxford Diffraction XtaLAB Synergy S diffractometer fitted with a Hypix6000HE hybrid photon counting detector and using Cu-Kα (l = 1.54184 Å) radiation.[1] Diffraction data were integrated, and absorption correction was applied using the CrysAlisPro software (Version 1.171.40.81a Rigaku Oxford Diffraction, 2020).[2] An empirical absorption correction using spherical harmonics was applied and implemented using the SCALE3 ABSPACK scaling algorithm. Crystal structures were solved using SHELXT[3] intrinsic phasing and refined against $|F^2|$ using ShelXL[4] through the Olex2 (1.5) interface.[3-5] Non-hydrogen atoms were refined with anisotropic displacement parameters. All samples were suspended in MiTeGen LVCO-5 Cryo Oil™.

Powder X-Ray diffraction

Powder X-ray diffraction (PXRD) patterns were measured using a Bruker D8 Advance Eco Diffractometer with Cu Kα radiation (λ = 1.54050 Å), operated in the 2θ range from 5° to 55° at room temperature (20-25 °C). The diffractometer was equipped with a 1000 W Cu-anode X-Ray source with Ni Kβ filter, vertical θ - 2θ goniometer, motorized divergence slits, and a LynxEye XE 1D energy discriminative strip detector. Data was analyzed in the DIFFRAC.SUITE package (DIFFRAC.EVA V6.0 Bruker), with crystallinity computed using the following formulae:

$$\%\ amorphous = \frac{global\ area - reduced\ area}{global\ area} \times 100\%$$

$$\%\ crystallinity = 100 - \%\ amorphous$$

Where

$$global\ area = total\ area\ of\ scan$$

$$reduced\ area = area\ of\ the\ whole\ scan\ subtracted\ by\ the\ background$$

UV-Vis absorbance spectroscopy

Solution-state absorbance spectra were collected on an Agilent Technologies Cary 60 UV-Vis spectrophotometer using Starna scientific 3.5 mL quartz cuvettes of 10 mm path length. Baseline corrections were applied over the entire collected wavelength range. Solvents were of spectroscopic grade.

Fluorescence spectroscopy

Steady-state fluorescence measurements were run on an Agilent Technologies Cary Eclipse fluorescence spectrophotometer with intensities corrected for detector efficiency. Thorlabs Macro Fluorescence cuvettes of 10 mm path length were used and fluorescence quantum yields were obtained using the comparative method, with quinine sulfate (0.546 in 0.5 M sulfuric acid) as the reference standard.[6] Inner filter effects were avoided by ensuring optical densities no greater than 0.1. Solid-state emission and excitation spectra were collected using an Agilent Technologies Cary Eclipse Fluorescence Spectrometer with an Agilent Cary Eclipse Solid Sample Holder. Samples were mounted on a silica disk. Total PLQY measurements for the four solid forms were conducted on an Edinburgh Instruments FLSP920 luminescence spectrometer with a continuous wave Xe lamp excitation source. An excitation wavelength of 330 nm was used for each sample. The solid samples were placed between two quartz plates and mounted in an integrating sphere. The uncertainty in the PLQY values is estimated at ±10%. Gated photoluminescence emission decays were measured using a pulsed Xe lamp with an excitation pulse duration of 2 µs, a pulse repetition rate of 100 Hz, a measurement delay of 0.1 ms, and a measurement gate of 9 ms. For each sample, an excitation wavelength of 330 nm was used and emission was measured from 500 nm.

Thermogravimetric analysis

TGA was conducted on a Mettler Toledo TGA thermogravimetric analyzer, heating from 25 – 600 °C at a ramp rate of 10 °C min^{-1} under a 20 mL min^{-1} flow of nitrogen.

Differential scanning calorimetry

DSC experiments were performed on a PerkinElmer 8000 DSC running Pyris software with a standard cell at a ramp rate of 10 °C min^{-1}. Three complete heating and cooling cycles were performed, with a 1-minute isothermal between each cycle. Aluminium pans were crimped.

Mass spectrometry

HRMS experiments were performed by the School of Chemistry at Monash University, Clayton on an Agilent Q-TOF 6540 mass spectrometer, using the electrospray technique and controlled via the MassHunter software package.

Crystal explorer

Finalized CIFs were inputted to the CrystalExplorer 21.5 program to calculate Hirshfeld surfaces and fingerprint plots using high resolution.[7] Interaction energies were calculated about a centrally selected molecule at the B3LYP/6-31G(d,p) level, scaled with benchmarked energy models.[8] A cluster of molecules within a radius of 3.8 Å was generated about the central molecule and all fragments were completed before the calculation of energies. Lattice energies were estimated by generating clusters with increasing radii until lattice energies converged to within 1 kJ/mol.

Computational methods

All Density Functional Theory (DFT) and time-dependent DFT (TD-DFT) calculations were carried out the Orca software suite.[9, 10] The ωB97X functional was used in all cases, as a suitable hybrid functional to describe both local and charge-transfer transitions.[11] The Pople-type split-valence double-ζ atomic-orbital basis set with polarisation functions on all atoms 6-31++G(d,p) was used in all calculations.[12, 13]

S2: Experimental

Synthesis and characterization

Chemicals were used as purchased without further purification. Bromobenzene was dried over 3 Å molecular sieves and degassed using standard laboratory procedures. The reactions were carried out under a nitrogen atmosphere.

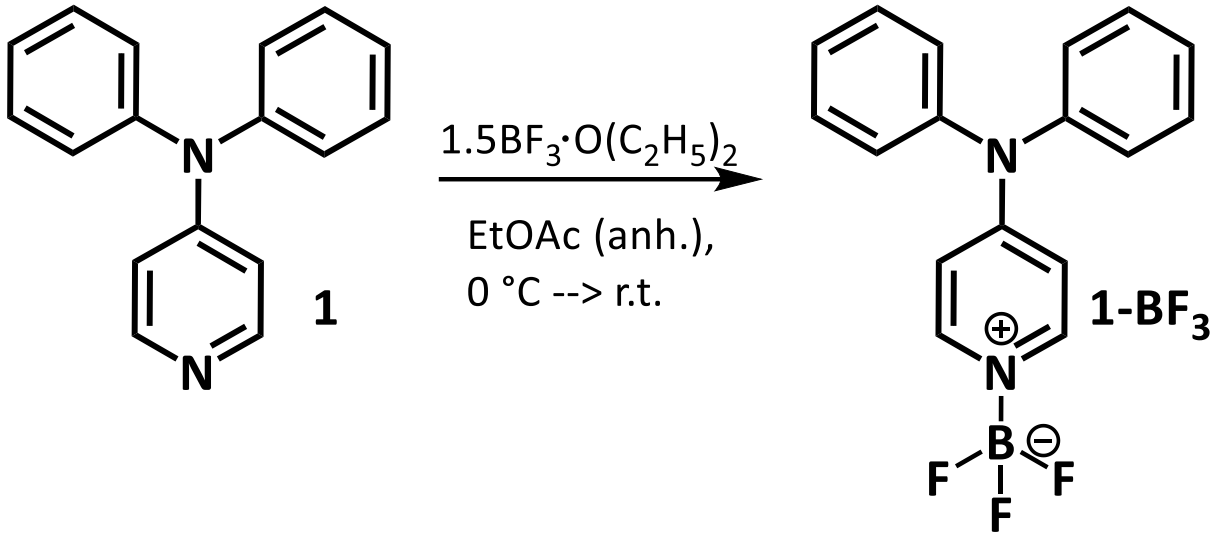

*Scheme S1 Synthetic pathway to **1-BF$_3$**.*

Synthesis of 1: The precursor N,N-diphenylpyridin-4-amine was prepared as reported previously.[14]

A suspension of 4-aminopyridine (1.00 g, 10.63 mmol), copper(I) iodide (300 mg, 1.57 mmol), potassium carbonate (2.80 g, 20.26 mmol), and 18-crown-6 (360 mg, 1.36 mmol) in anhydrous bromobenzene (25 mL) was stirred under a nitrogen atmosphere at 150 °C for 20 h. The reaction mixture was allowed to cool to room temperature and worked up with saturated NH_4Cl solution (~140 mL) and extracted with diethyl ether (3 × 50 mL). The combined organic phases were dried over $MgSO_4$, concentrated *in vacuo* and the resulting crude was purified by silica gel flash chromatography (dichloromethane/methanol, gradient 0-10 % methanol, product elutes in 5%) to afford the product as a colourless solid (1.327 g, 51%, m.p. 116.1-117.1 °C).

R_f: 0.55 (9:1, dichloromethane/methanol).

FT-IR (neat): υ_{max} 3089, 3027, 2650, 2530, 2477, 2372, 2342, 2323, 2115, 2083, 2057, 1874, 1660, 1629, 1574, 1544, 1482, 1451, 1425, 1336, 1304, 1265, 1238, 1217, 1188, 1167, 1074, 1025, 987, 942, 904, 837, 811, 775, 758, 736, 720, 699 cm^{-1}.

Elemental Analysis (%) calculated (found): C, 82.90 (82.91); H, 5.73 (5.81); N, 11.37 (11.11).

δ_H (600 MHz; $CDCl_3$): 8.23 (d, *J* = 4.7 Hz, 2H), 7.41 – 7.30 (m, 4H), 7.23 – 7.15 (m, 6H), 6.74 (d, *J* = 4.7 Hz, 2H).

δ_C (151 MHz; $CDCl_3$): 154.01, 149.78, 145.19, 129.95, 126.80, 125.81, 112.76.

HRMS (ESI-TOF) *m/z* [$(M + H)^+$] calcd. for $C_{17}H_{15}N_2$ 247.1230, found 247.1230.

Synthesis of 1-BF$_3$: 4-(diphenylamino)pyridin-1-iumtrifluoroborate

To a stirred solution of **1** (200 mg, 0.8 mmol) in anhydrous ethyl acetate (4 mL) under an inert atmosphere at 0 °C was added boron trifluoride diethyl etherate (150 µL,1.2 mmol) slowly. After stirring at 0 °C for 15 minutes a colourless precipitate formed. The suspension was slowly brought to room temperature and stirred for a further 15 minutes before being quenched with $Na_2CO_{3(sat)}$ and extracted with dichloromethane (3 × 5 mL). The combined organic phases were washed with brine (2 x 5mL), dried over $MgSO_4$, concentrated *in vacuo* and the resulting crude was purified by flash chromatography (dichloromethane) to afford the product (168 mg, 66%, m.p. 174-180 °C) as a colourless solid.

R_f: 0.42 (dichloromethane).

FT-IR (neat): ν_{max} 3130, 3085, 3061, 3039, 2962, 2925, 2903, 2853, 2753, 2610, 2367, 2345, 2331, 2325, 1644, 1594, 1561, 1544, 1527, 1512, 1492, 1475, 1459, 1453, 1438, 1432, 1421, 1378, 1342, 1313, 1305, 1284, 1278, 1259, 1224, 1204, 1189, 1166, 1143, 1100, 1087, 1042, 1028, 1004, 978, 972, 965, 951, 939, 932, 918, 903, 888, 852, 845, 831, 778, 760, 742, 735, 708, 703, 695, 677, 663 cm^{-1}.

Elemental Analysis (%) calculated (found): C, 65.00 (65.34); H, 4.49 (4.44); N, 8.92 (8.83).

δ_H (400 MHz; CD_2Cl_2): 8.10 (d, *J* = 5.3 Hz, 2H), 7.54-7.45 (m, 4H), 7.43-7.34 (m, 2H), 7.34-7.26 (m, 4H), 6.77 (d, *J* = 7.6 Hz, 2H).

δ_C (151 MHz; CD_2Cl_2): 157.65, 143.16, 143.01, 130.95, 128.46, 127.59, 110.79.

δ_F (376 MHz; CD_2Cl_2): -152.11 (dt, *J* = 26.4, 13.8 Hz).

δ_B (376 MHz; CD_2Cl_2): 0.23 (q, *J* = 13.1 Hz).

HRMS (ESI-TOF) *m/z* [$(M + NH_4)^+$] calcd. for $C_{17}H_{18}F_3N_3B$ 332.1546, found 332.1552, *m/z* [$(M + Na)^+$] calcd. for $C_{17}H_{14}F_3N_2BNa$ 337.1100, found 337.1107.

S3: NMR spectra

^{1}H NMR

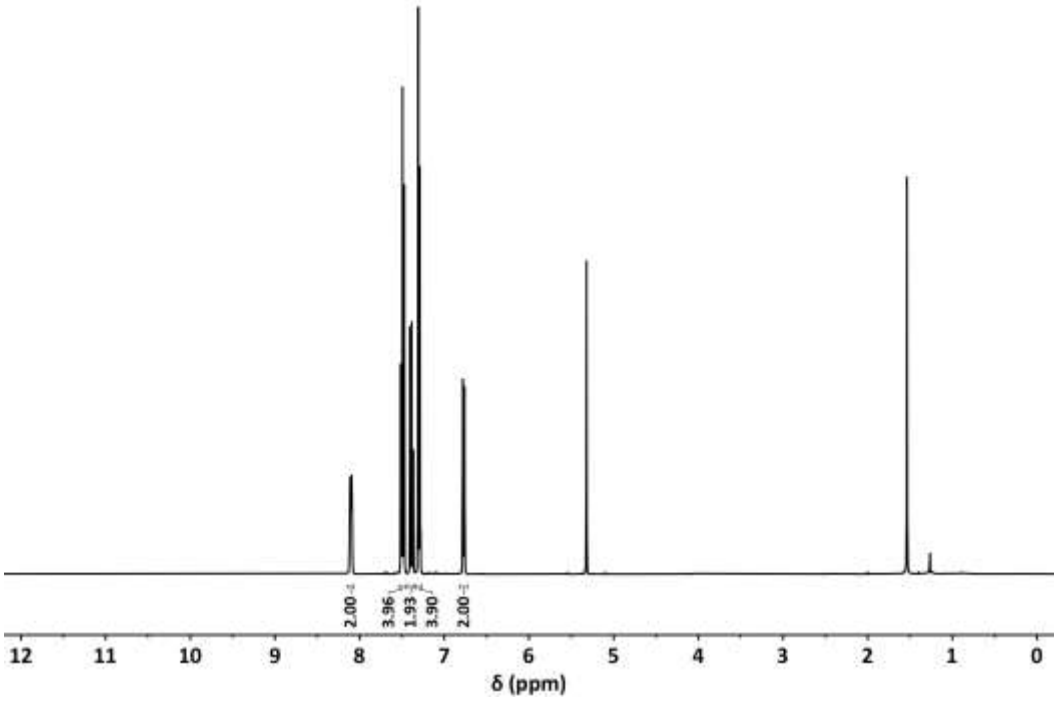

*Figure S1 ^{1}H NMR for **1-BF_3** in CD_2Cl_2.*

^{13}C NMR

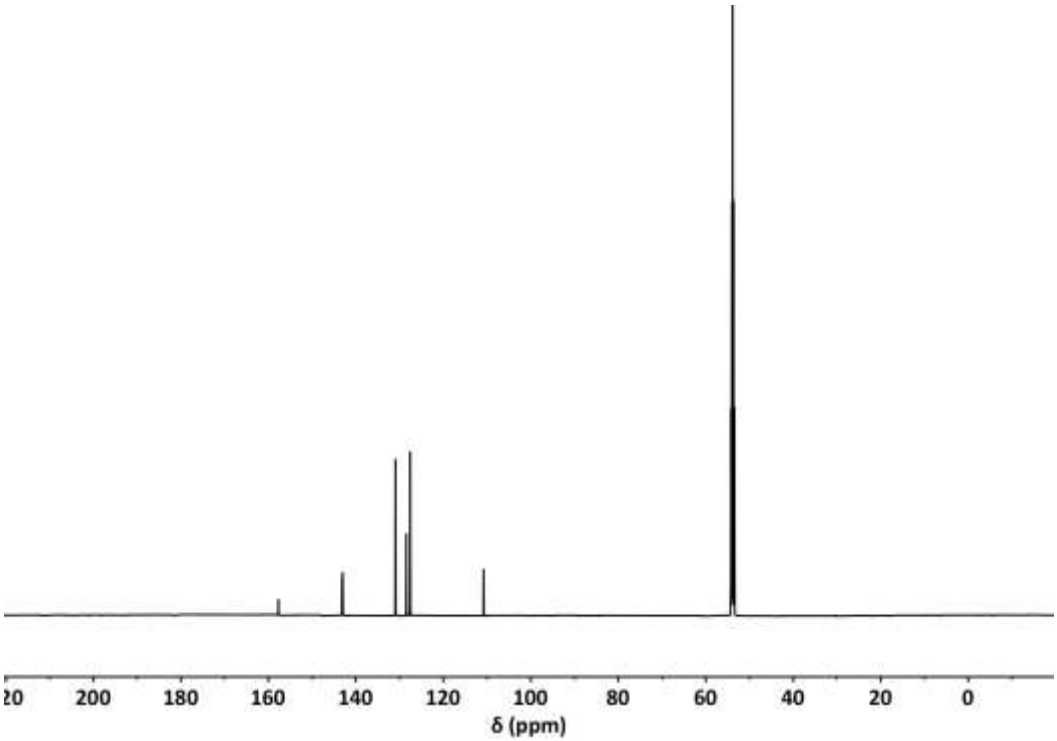

*Figure S2 ^{13}C NMR for **1-BF_3** in CD_2Cl_2.*

^{11}B NMR

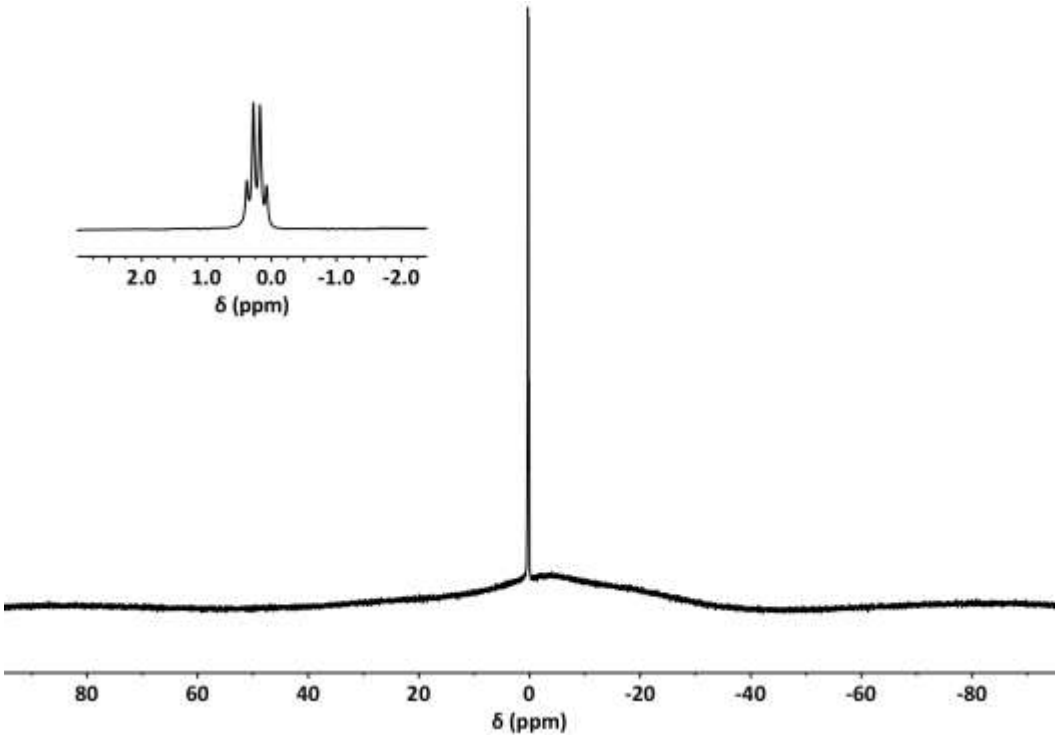

*Figure S3 ^{11}B NMR for **1-BF$_3$** in CD_2Cl_2.*

^{19}F NMR

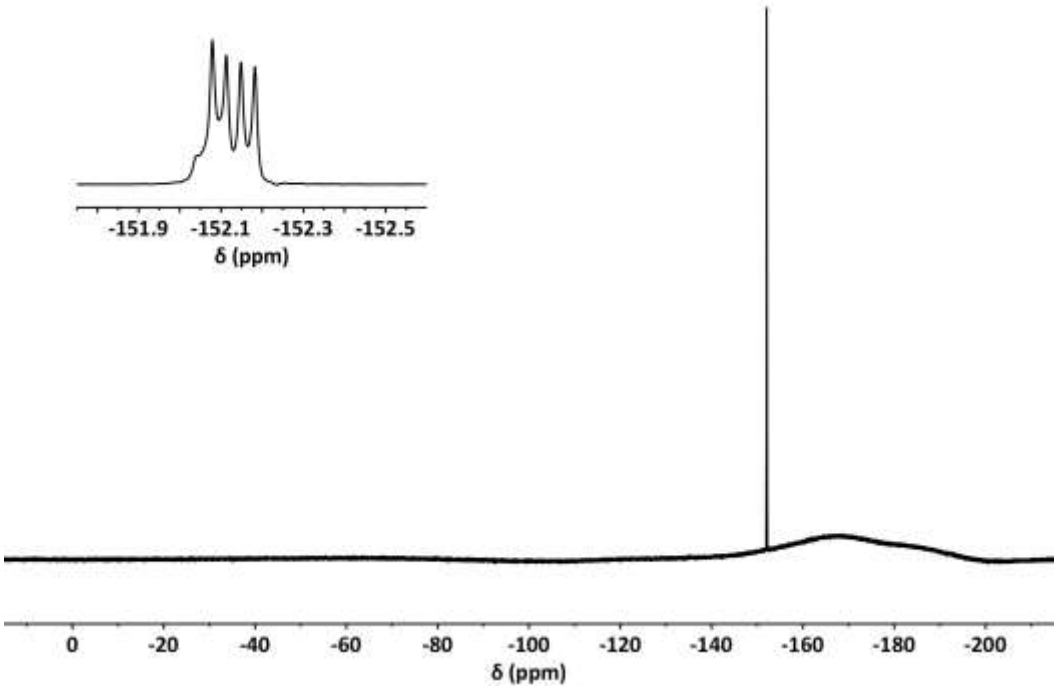

*Figure S4 ^{19}F NMR for **1-BF$_3$** in CD_2Cl_2.*

S4: Crystallographic details

Crystallographic information files are freely available via Deposition Numbers 2310937, 2310938 and 2310950 in the Cambridge Crystallographic Data Centre.

*Table S1 Crystallographic details for compounds **1-BF_3** at 123 and 293 K and **1H-BF_4**.*

	1-BF_3 123 K	**1-BF_3 293 K**	**1H-BF_4**
Identification code	PM3_20_DCM	PM3_42_DCM	PM3_18_THF
Empirical formula	$C_{34}H_{28}B_2F_6N_4$	$C_{34}H_{28}B_2F_6N_4$	$C_{17}H_{15}BF_4N_2$
Formula weight	628.22	628.22	334.12
Temperature/K	123.00(10)	293	123.01(10)
Crystal system	triclinic	triclinic	monoclinic
Space group	P-1	P-1	$P2_1$
a/Å	8.3590(2)	8.48980(10)	10.30620(10)
b/Å	11.6452(2)	11.7179(2)	7.70180(10)
c/Å	16.1214(3)	16.2792(2)	10.32470(10)
α/°	90.762(2)	90.7320(10)	90
β/°	100.271(2)	99.9450(10)	101.0560(10)
γ/°	94.709(2)	95.1060(10)	90
Volume/Å^3	1538.31(5)	1588.18(4)	804.326(15)
Z	2	2	2
ρ_{calc}g/cm^3	1.356	1.314	1.380
μ/mm^{-1}	0.889	0.861	0.974
F(000)	648.0	648.0	344.0
Crystal size/mm^3	0.05 × 0.14 × 0.24	0.03 × 0.08 × 0.36	0.12 × 0.16 × 0.32
Radiation	Cu Kα (λ = 1.54184)	Cu Kα (λ = 1.54184)	Cu Kα (λ = 1.54184)
2Θ range for data collection/°	7.62 to 160.664	7.578 to 160.8	8.726 to 159.92
Index ranges	-10 ≤ h ≤ 10, -13 ≤ k ≤ 14, -20 ≤ l ≤ 20	-10 ≤ h ≤ 10, -14 ≤ k ≤ 14, -20 ≤ l ≤ 17	-9 ≤ h ≤ 12, -9 ≤ k ≤ 9, -13 ≤ l ≤ 13
Reflections collected	31806	33408	13391
Independent reflections	6373 [R_{int} = 0.0297, R_{sigma} = 0.0200]	6808 [R_{int} = 0.0490, R_{sigma} = 0.0389]	3393 [R_{int} = 0.0324, R_{sigma} = 0.0254]
Data/restraints/parameters	6373/0/416	6808/0/416	3393/1/222
Goodness-of-fit on F^2	1.068	1.142	1.067
Final R indexes [I>=2σ (I)]	R_1 = 0.0363, wR_2 = 0.0982	R_1 = 0.0533, wR_2 = 0.1413	R_1 = 0.0321, wR_2 = 0.0832
Final R indexes [all data]	R_1 = 0.0405, wR_2 = 0.1006	R_1 = 0.0663, wR_2 = 0.1468	R_1 = 0.0328, wR_2 = 0.0839
Largest diff. peak/hole / e Å^{-3}	0.24/-0.27	0.36/-0.37	0.15/-0.18
Flack parameter	NA	NA	-0.01(5)

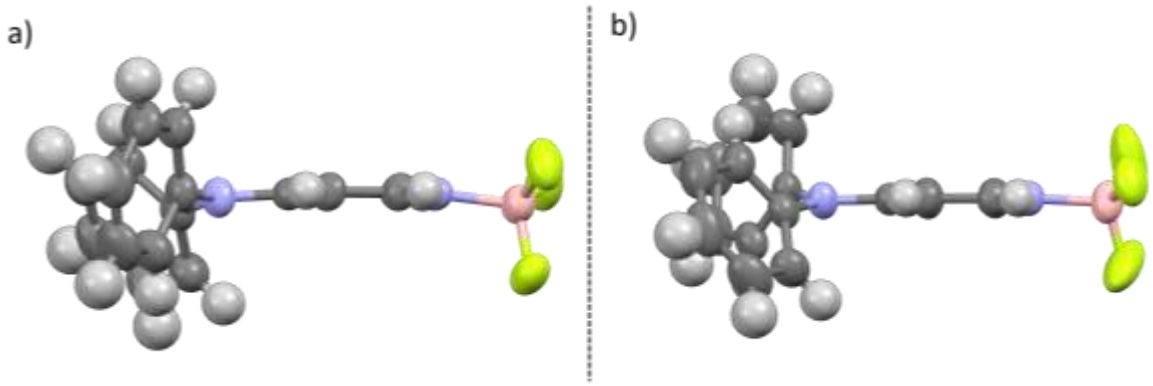

Figure S5 Two distinct molecules making up the asymmetric unit of ***1-BF₃ 293 K****. Puckering along the N_1-C_1-N_2-B axis can be seen in a) that is not present in b).*

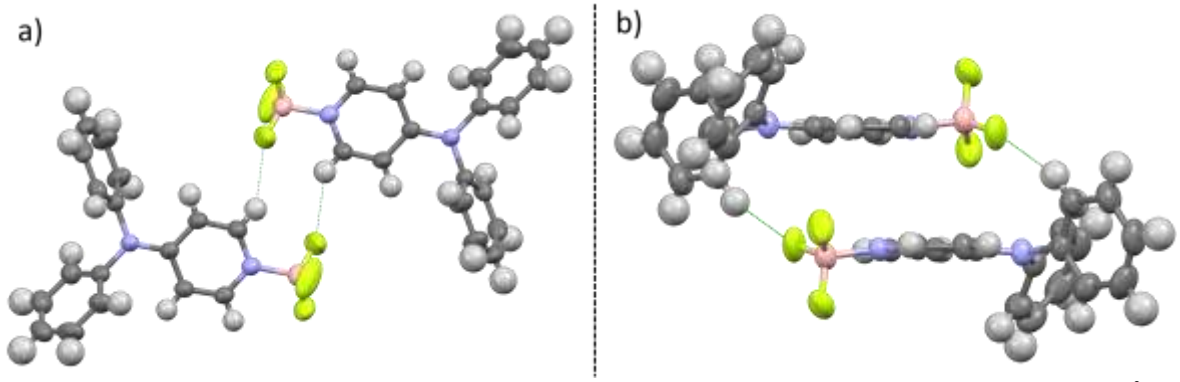

Figure S6 Key intermolecular distances/calculated interactions energies in ***1-BF₃ 293 K*** *a) side on dimer 2.4433(17) Å/45.0 kJ/mol and b) offset stacked dimer with 2.4358(12) Å/83.9 kJ/mol.*

S5: Thermogravimetric analysis

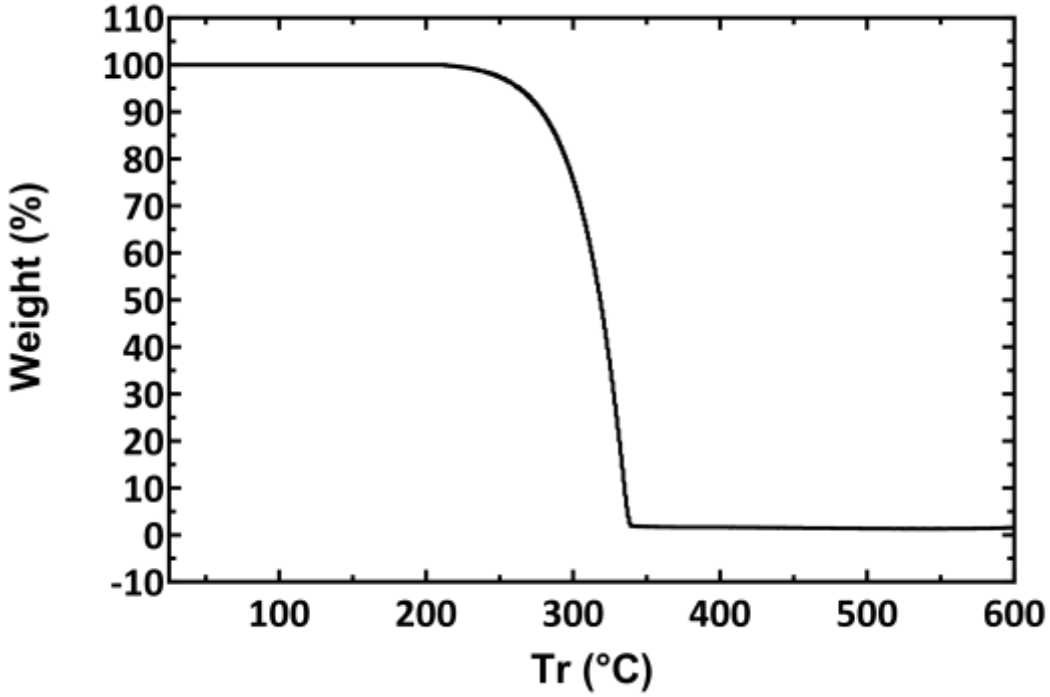

*Figure S7 Thermogravimetric analysis for **1-BF_3** with decomposition onset at 215 °C and complete decomposition by 338 °C.*

S6: Differential scanning calorimetry

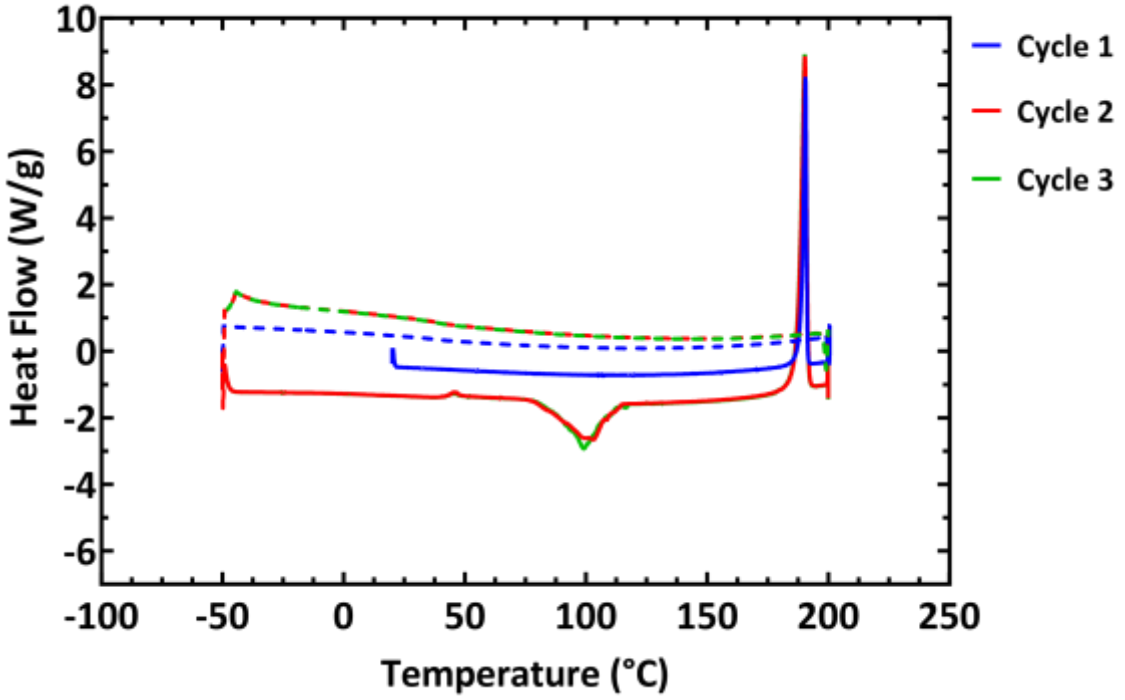

*Figure S8 Differential scanning calorimetry of **1-BF_3** showing a melting point peak at 190.55 °C (approximate enthalpy of fusion 92 J/g) and curing phase transition peaks between 85-109 °C (approximate enthalpy of -64 J/g) on the second and third heating cycles. Three scan cycles are shown with exo down.*

S7: Solid-state luminescence data

*Table S2 Solid-state photophysical data for **1-BF_3**.*

Sample form	$\lambda_{max,Fl}$ (nm)	$\lambda_{max,Phos}$ (nm)
C	412	486
G 320	416	485
G 360	465	485*
F	411	481
An	413	500

* **G 360** is the same sample as **G 320** and has the same $\lambda_{max,Phos}$.

Solid state phosphorescence excitation and emission spectra

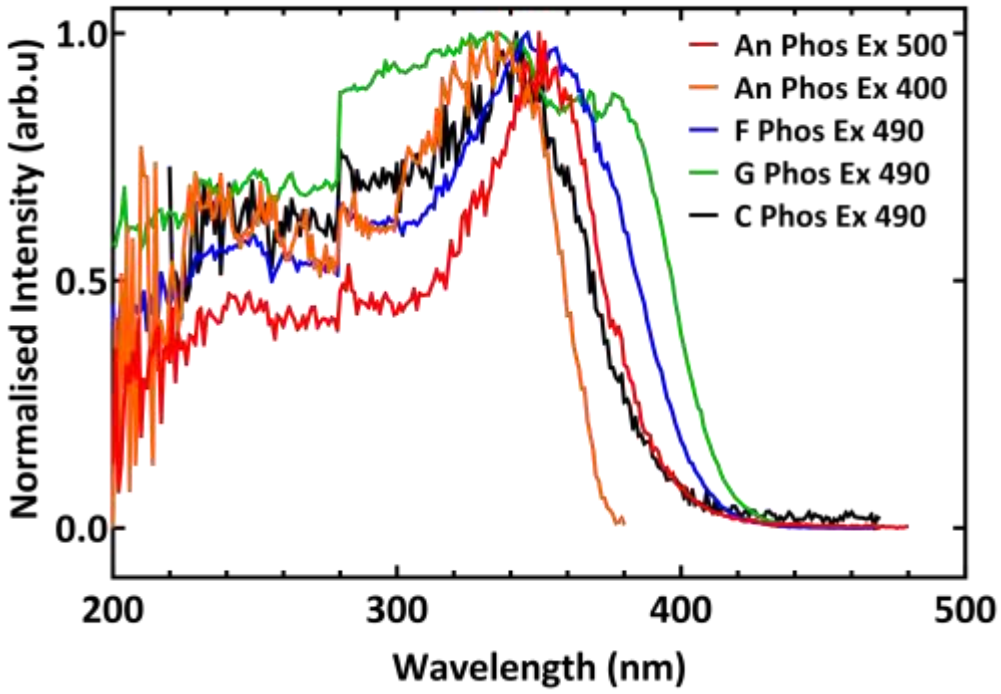

Figure S9 Solid state phosphorescence excitation spectra.

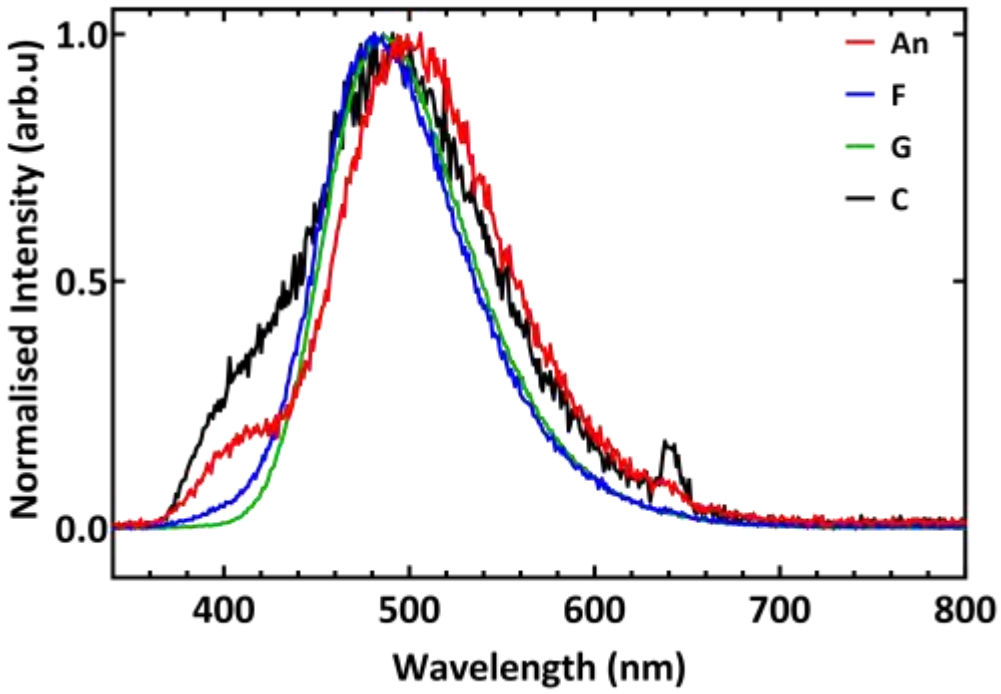

Figure S10 Solid-state phosphorescence spectra.

Time-resolved phosphorescence decay profiles

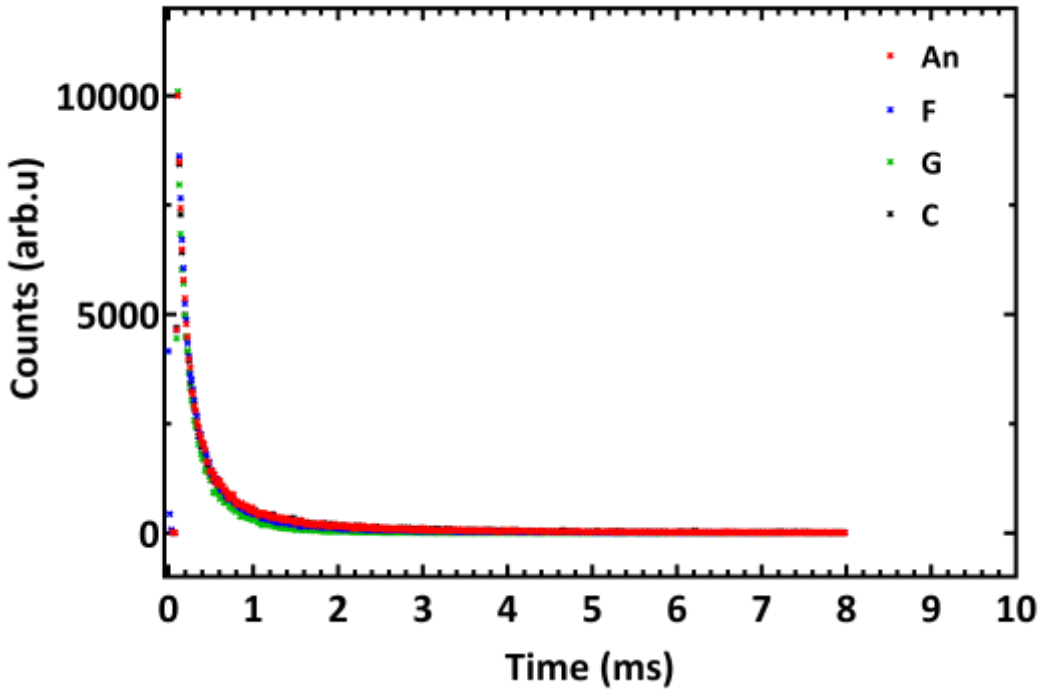

Figure S11 Phosphorescence decays profiles on a linear count scale.

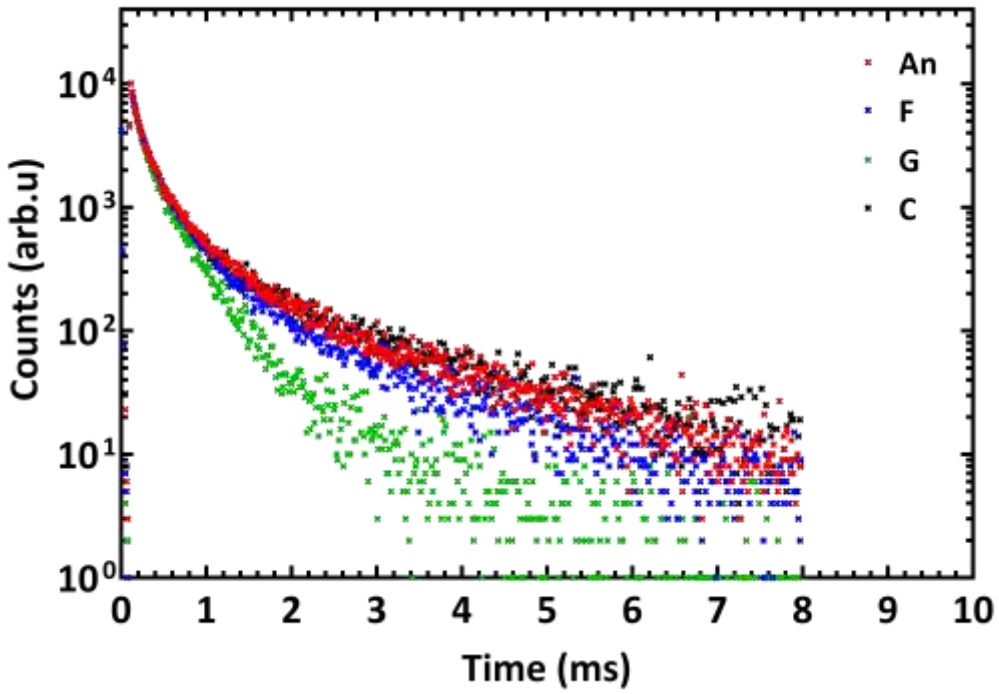

Figure S12 Phosphorescence decay profiles with counts on a logarithmic scale.

Solid state fluorescence excitation and emission spectra

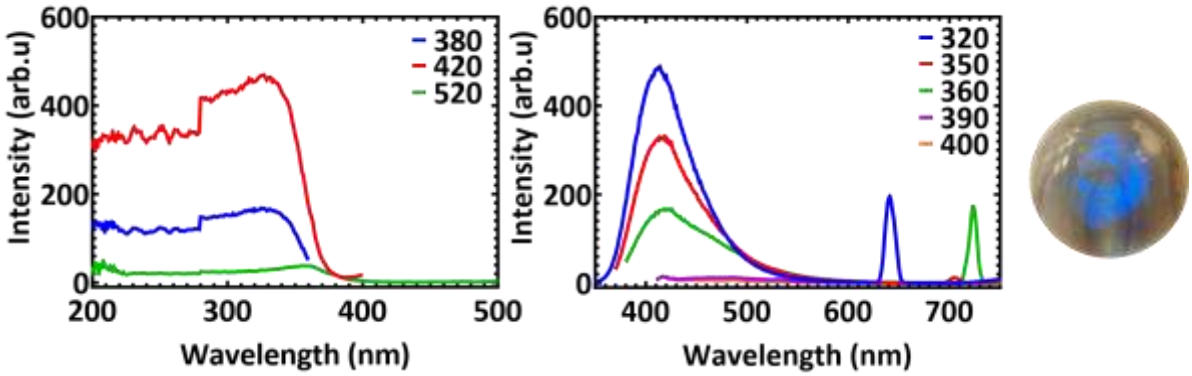

*Figure S13 Excitation and emission spectra for **1-BF₃** after annealing the **G** form at 110 °C for 1 hour.*

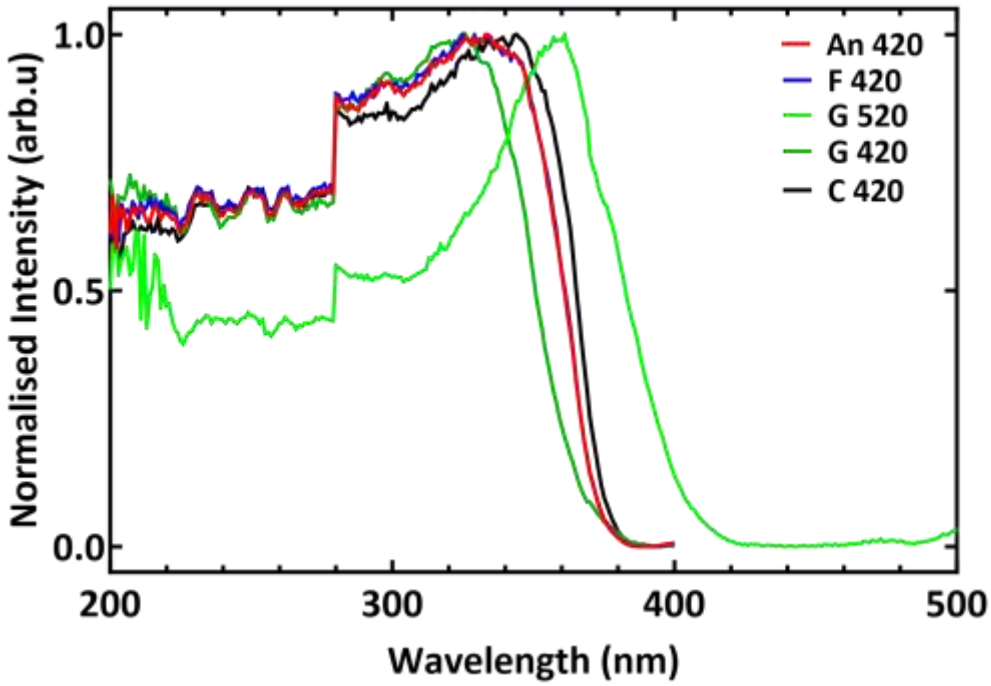

Figure S14 Normalized solid-state excitation spectra in four physical forms.

S8: Powder X-Ray diffraction

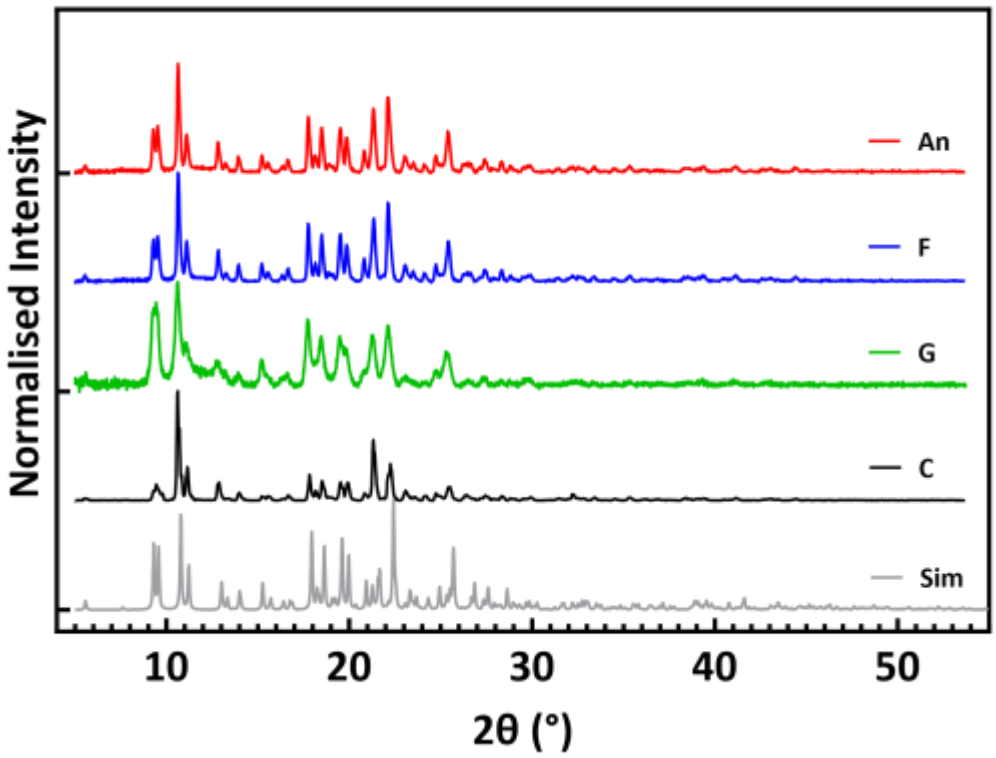

*Figure S15 PXRD patterns for **1-BF_3** in four physical forms and simulated pattern from structure collected at 293 K.*

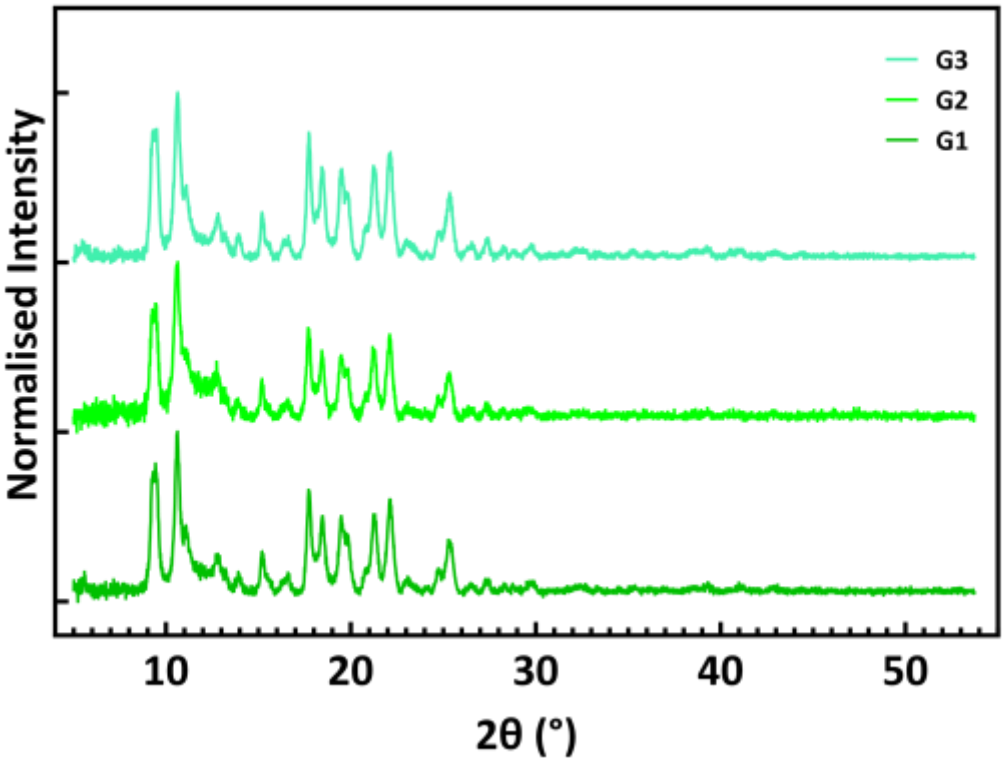

*Figure S16 PXRD patterns for **1-BF_3** after grinding for 5 **(G1)**, 10 **(G2)** and 20 **(G3)** minutes.*

Table S3 Computed crystallinity values for the four physical forms.

Sample form	% crystalline	% amorphous
C	85.6	14.4
G1	51.9	48.1
G2	44.1	55.9
G3	55.5	44.5
F	79.2	20.8
An	76.4	23.6

S9: Mechanofluorochromism NMR study

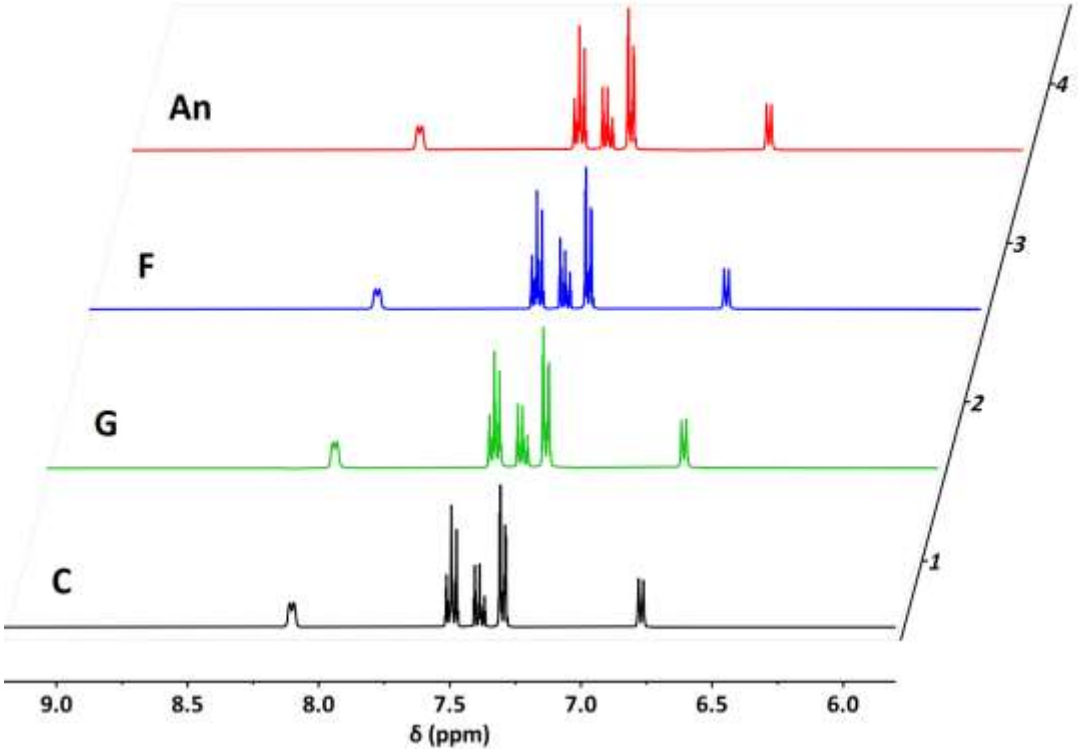

*Figure S17 ^{1}H NMR in four forms for **1-BF_3**.*

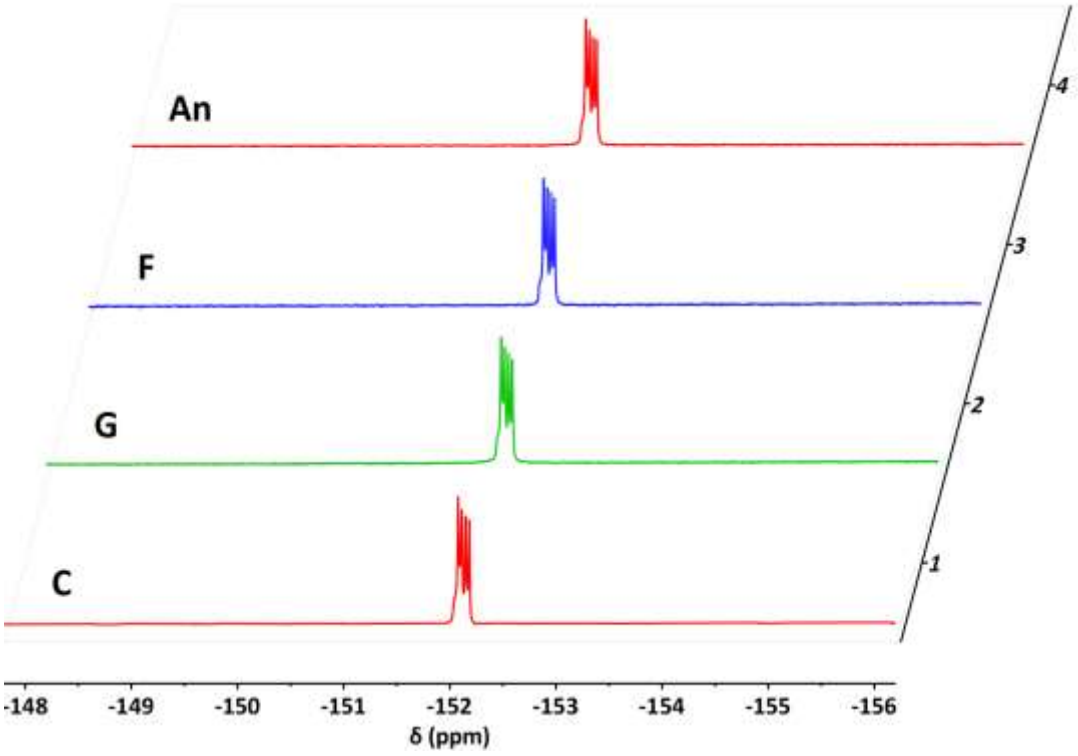

*Figure S18 ^{19}F NMR in four forms for **1-BF_3**.*

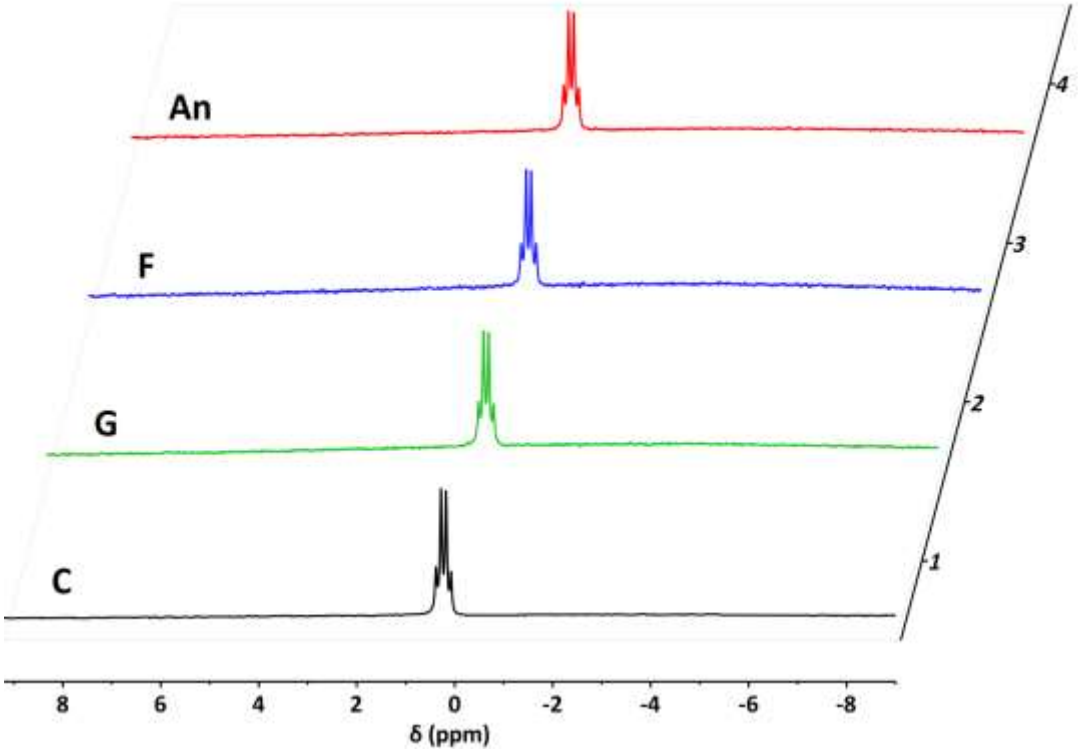

*Figure S19 ^{11}B NMR in four forms for **1-BF_3**.*

S10: FT-IR spectra

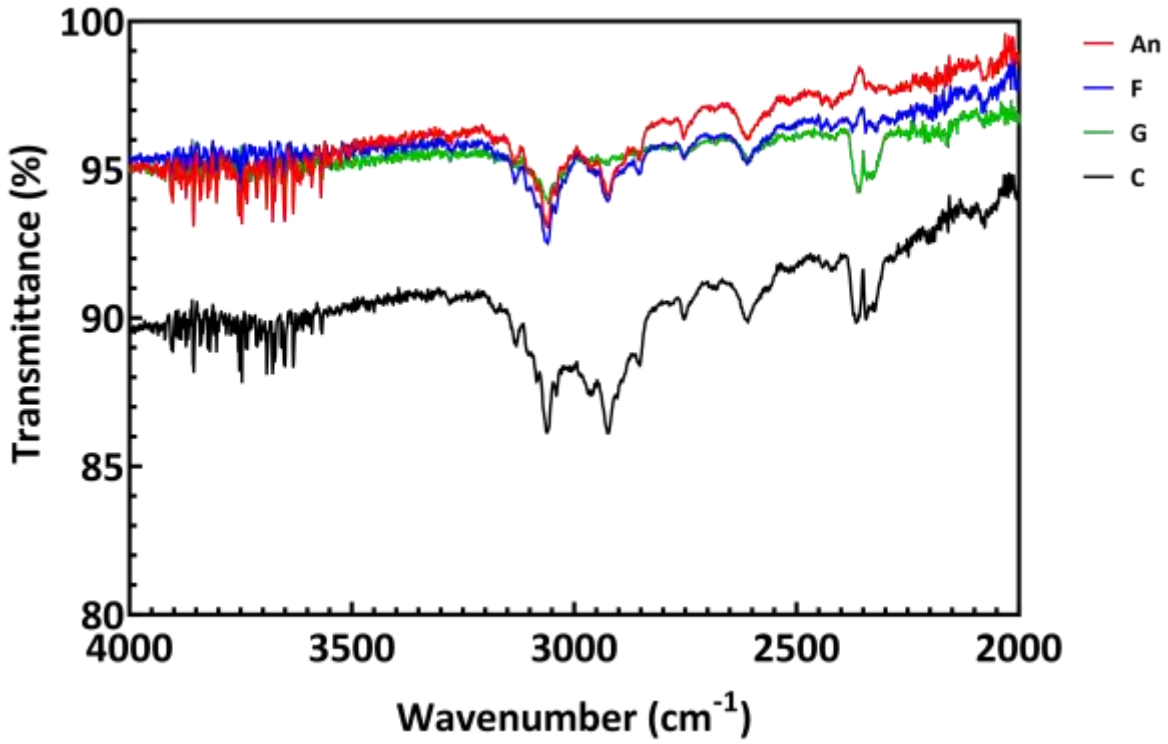

*Figure S20 FT-IR spectra for four forms of **1-BF$_3$** from 4000 to 2000 cm^{-1}.*

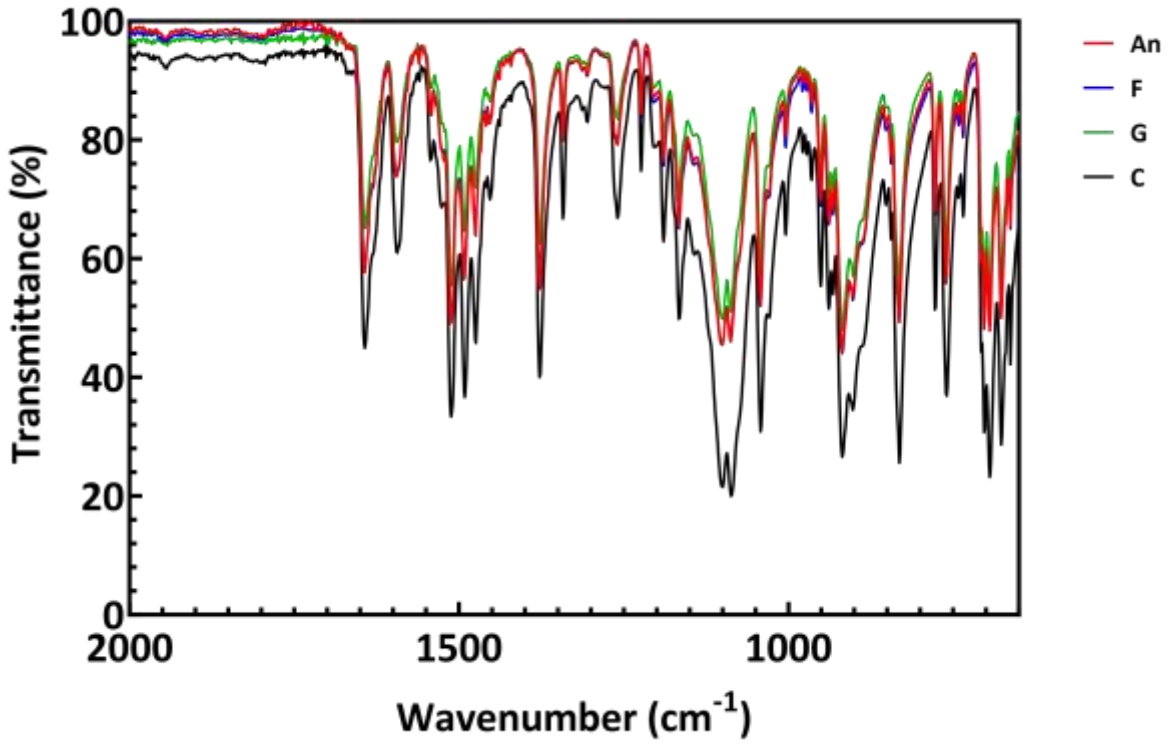

*Figure S21 FT-IR spectra for four forms of **1-BF$_3$** from 2000 to 650 cm^{-1}.*

S11: Solution-state luminescence excitation and emission data

*Table S4 Solution-state photophysical data for **1-BF_3**.*

Solvent	$\lambda_{max,Abs}$ (nm)	$\lambda_{max,Fl}$ (nm)	ε ($M^{-1}\cdot cm^{-1}$)	Φ_{Fl}
Toluene	303	488	9710	0.12
DCM	298	546	11920	0.06
MeOH	289	577	12330	<0.01
ACN	288	582	14050	<0.01

Solution state absorbance and excitation spectra

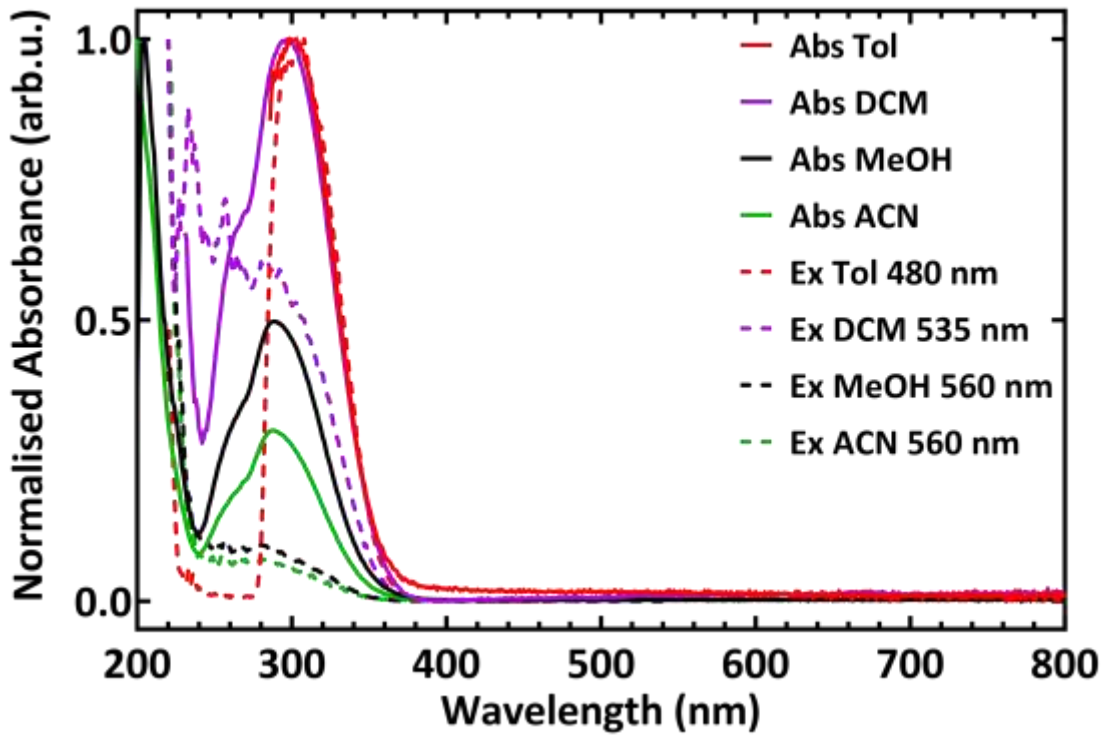

*Figure S22 Overlay of excitation and absorbance spectra for **1-BF_3**.*

Solution state emission spectra

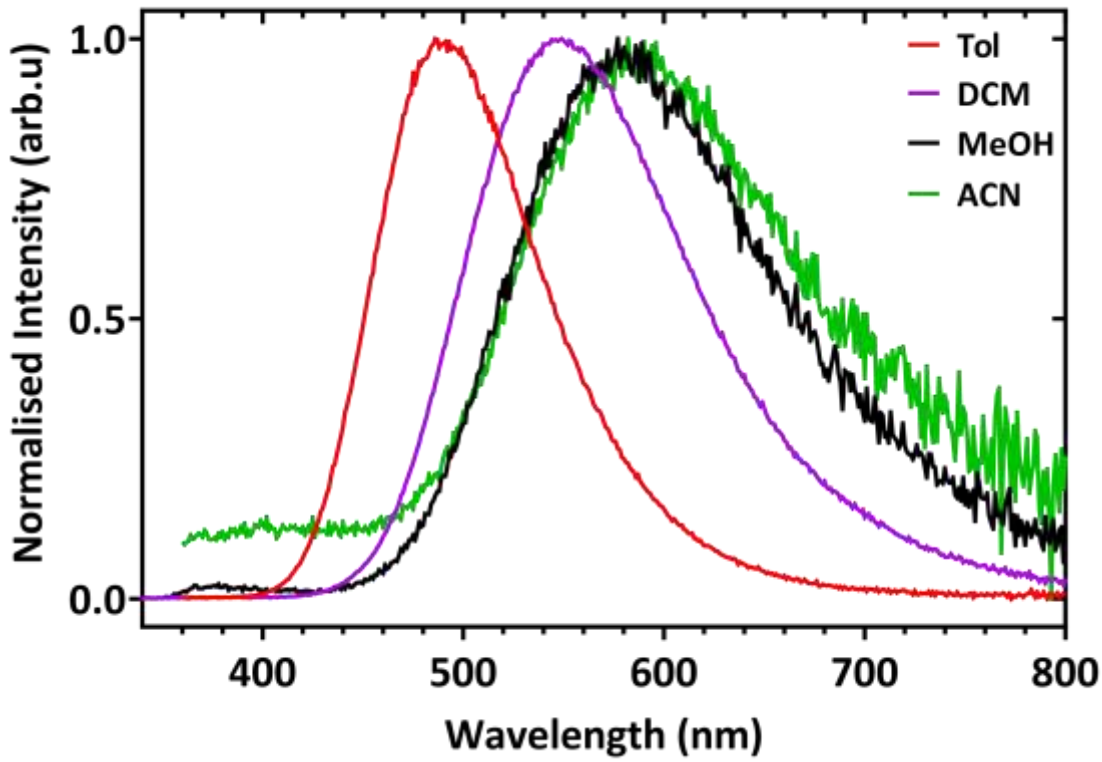

Figure S23 Normalized solution state emission spectra for ***1-BF$_3$.***

S12: Quantum chemical calculations

*Table S5 Ground state optimized geometry DFT and TD-DFT parameters for **1-BF_3**.*

Medium	Vertical transition energy **(nm)**	Oscillator strength (f)	Transition character	GS dipole moment **(Debye)**
Gas Phase	258.7	0.668	87.6% HOMO→LUMO	12.29
Tol	249.5	0.697	86.0% HOMO→LUMO	14.09
DCM	246.1	0.709	84.9% HOMO→LUMO	15.22
ACN	245.1	0.714	84.4% HOMO→LUMO	15.56
MeOH	245.1	0.710	84.5% HOMO→LUMO	15.54

*Table S6 Excited state optimized geometry TD-DFT parameters for **1-BF_3**.*

Medium	Vertical transition energy **(nm)**	Oscillator strength (f)	Transition character	ES dipole moment **(Debye)**
Gas Phase	402.0	0.040	91.2% HOMO←LUMO	19.26
Tol	386.8	0.111	91.2% HOMO←LUMO	21.88
DCM	382.0	0.199	91.4% HOMO←LUMO	23.40
ACN	382.2	0.239	91.5% HOMO←LUMO	23.74
MeOH	381.8	0.239	91.5% HOMO←LUMO	23.71

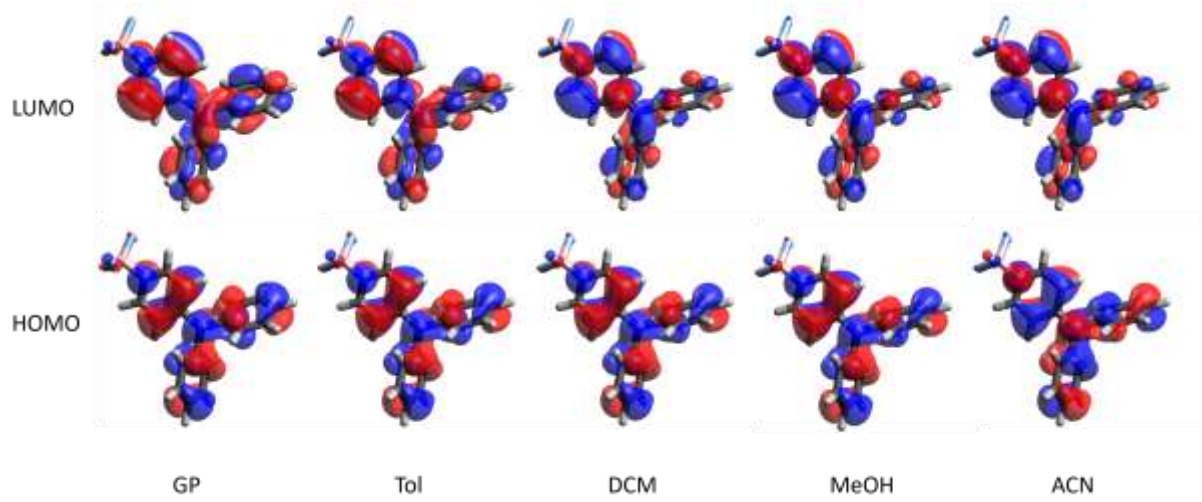

Figure S24 ωB97X/6-31++G(d,p) o*rbitals (plotted with Avogadro) for the ground state optimized geometries of* ***1-BF₃*** *(isosurface value 0.02).*

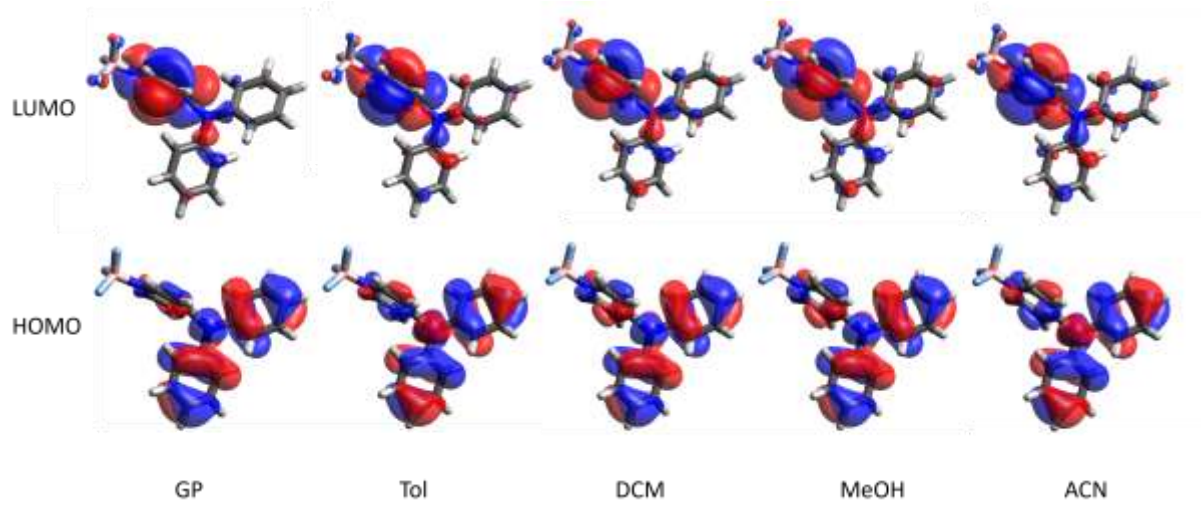

Figure S25 ωB97X/6-31++G(d,p) o*rbitals (plotted with Avogadro) for the first excited singlet state of* ***1-BF₃*** *(isosurface value 0.02).*

S13: References

1. P. Le Magueres, E. W. Reinheimer, M. Meyer, A. Jones and D. Kucharczyk, *Acta Crystallographica Section A*, 2018, **74**, a468.
2. CrysAlisPRO, Oxford Diffraction /Agilent Technologies UK Ltd, Yarnton, England.
3. G. Sheldrick, *Acta Crystallographica Section A*, 2015, **71**, 3-8.
4. G. Sheldrick, *Acta Crystallographica Section C*, 2015, **71**, 3-8.
5. O. V. Dolomanov, L. J. Bourhis, R. J. Gildea, J. A. K. Howard and H. Puschmann, *J. Appl. Crystallogr.*, 2009, **42**, 339-341.
6. W. H. Melhuish, *J. Phys. Chem.*, 1961, **65**, 229-235.
7. P. R. Spackman, M. J. Turner, J. J. McKinnon, S. K. Wolff, D. J. Grimwood, D. Jayatilaka and M. A. Spackman, *J. Appl. Crystallogr.*, 2021, **54**, 1006-1011.
8. C. F. Mackenzie, P. R. Spackman, D. Jayatilaka and M. A. Spackman, *IUCrJ*, 2017, **4**, 575-587.
9. F. Neese, *WIREs Computational Molecular Science*, 2012, **2**, 73-78.
10. F. Neese, *WIREs Computational Molecular Science*, 2018, **8**, e1327.
11. J.-D. Chai and M. Head-Gordon, *J. Chem. Phys.*, 2008, **128**, 084106.
12. R. Ditchfield, W. J. Hehre and J. A. Pople, *J. Chem. Phys.*, 1971, **54**, 724-728.
13. W. J. Hehre, R. Ditchfield and J. A. Pople, *J. Chem. Phys.*, 1972, **56**, 2257-2261.
14. J. Gamboa Varela, A. De Chatterjee, P. Guevara, V. Ramirez, A. J. Metta-Magaña, D. Villagrán, A. Varela-Ramirez, S. Das and J. E. Nuñez, *J. Biol. Inorg. Chem.*, 2014, **19**, 967-979.